BRNO UNIVERSITY OF TECHNOLOGY
VYSOKÉ UČENÍ TECHNICKÉ V BRNĚ

FACULTY OF MECHANICAL ENGINEERING
FAKULTA STROJNÍHO INŽENÝRSTVÍ

INSTITUTE OF PHYSICAL ENGINEERING
ÚSTAV FYZIKÁLNÍHO INŽENÝRSTVÍ

ROLE OF THERMAL NEAR FIELD IN CRYOGENIC RAYLEIGH-BÉNARD CONVECTION
STUDIUM VLIVU TEPELNÉHO BLÍZKÉHO POLE NA KRYOGENNÍ RAYLEIGHOVU-BÉNARDOVU KONVEKCI

BACHELOR'S THESIS
BAKALÁŘSKÁ PRÁCE

AUTHOR   TOMÁŠ VĚŽNÍK
AUTOR PRÁCE

SUPERVISOR   Ing. PAVEL URBAN, Ph.D.
VEDOUCÍ PRÁCE

BRNO 2019

Abstract

This bachelor thesis is focused on the effect of the thermal near field (NF) radiation on
(i) the onset of Rayleigh-Bénard convection (RBC) and (ii) the thermal influence on the
temperature sensors used in RBC studies. In the first part, the theoretic base for both
studied areas, RBC and NF, is presented. Further, the ways of finding the onset of RBC,
the temperature profiles, the basic equations for heat transfer in far field and near field
and the description of the apparatus used for the measurements of radiative heat transfer
are given too. In the practical part, the process of measurement is presented and the
model that we obtained for describing the dependence of the coefficient of radiative heat
transfer between two Cu surfaces is demonstrated. Afterwards, the data are used to
analyse the effect of NF on the onset of convection, and to calculate the influence on the
temperature profile measurements with cryogenic temperature sensors and, at last, the
comparison of total heat transferred over the experimental cell with NF heat transfer over
the thermal boundary layers arising in RBC is done. A goal of this thesis was to find out
whether the effect of NF can explain the contradictory results of determining the onset
of convection in cryogenic RBC (expressed by critical Ra_c) based on the measurements
of the heat transfer in RBC and of the effectivity of heat transfer at high values of Ra
numbers in cryogenic experiments. The current evaluations clearly demonstrate that the
effect of NF on studied phenomena is by several orders of magnitude smaller than other
relevant effects and can thus justly be neglected.

Abstrakt

Tato bakalářská práce se zabývá vlivem tepelného záření v blízkém poli (near field - NF) na
(i) nástup Rayleighovy-Bénárdovy konvekce (RBC) a (ii) tepelným ovlivněním teplotních
snímačů zářením v blízkém poli používaných pro studium RBC. V první části je uveden
teoretický základ pro obě dvě zkoumané oblasti, RBC a NF. Jsou zde uvedeny způsoby
zjišťování nástupu RBC, teplotní profily v RBC, základní vztahy pro přenos tepla zářením
a popis použité aparatury pro měření přenosu tepla zářením. V praktické části je uveden
postup měření a je prezentován získaný model pro popis závislosti koeficientu přenosu
tepla zářením mezi dvěma měděnými povrchy. Následně jsou získaná data použita pro
analýzu vlivu NF na nástup konvekce, je spočítán vliv na měření teplotních profilů kryo-
genními teplotními snímači a nakonec je provedeno srovnání celkového přeneseného tepla
experimentální celou s přenosem tepla prostřednictvím NF přes teplotní mezní vrstvy
vznikající v RBC. Cílem bylo zjistit, zda by vliv NF mohl vysvětlit rozporné výsledky
kryogenních experimentů při určení nástupu konvekce v RBC (kritického Ra_c) na základě
měření přenosu tepla v RBC a v efektivitě teplného přenosu za vysokých hodnot Ra čísla.
Z vyhodnocení vyplývá, že efekt NF na studované jevy je zanedbatelně malý.

Keywords

Rayleigh-Bénard convection, thermal near field, critical Rayleigh number, onset of con-
vection, temperature profiles measurement

Klíčová slova

Rayleighova-Bénardova konvekce, tepelné blízké pole, kritické Rayleighovo číslo, nástup
konvekce, měření teplotních profilů

VĚŽNÍK, T.*Role of thermal near field in cryogenic Rayleigh-Bénard convection.* Brno: Vysoké učení technické v Brně, Faculty of Mechanical Engineering, 2019. 35 s. Vedoucí Ing. Pavel Urban, Ph.D.

I declare that this bachelor thesis is based on my own work, led by my Bachelor's thesis supervisor Ing. Pavel Urban, Ph.D., and all utilized sources are properly listed in the bibliography. I proclaim that all presented information is accurate.

Tomáš Věžník

Contents

Introduction

Heat transfer and fluid flow as a result of natural convection are subject of interest in many diverse branches of science and technology. It affects the weather by a circulation of the air in the atmosphere, it moves the big masses of the water inside the oceans and the mantle under the surface of Earth or it can be used as a part of cooling fan.

Laboratory modelling of natural convection is possible on the base of a simplified physical model system - Rayleigh-Bénard convection (RBC). RBC is realized in a layer of working fluid often confined to a cylindrical experimental cell heated from below and cooled from above (see Figure 1.1).

RBC experiments with gaseous or liquid helium helium at cryogenic temperatures are known for their small sizes of the experimental cell and still reaching high Rayleigh numbers Ra which allow them to study very intensive turbulent flows. This is due to a strong dependence of He properties on temperature T and pressure p, especially near the critical point. It allows us to study a wide range of Ra too. However, there are many cryogenic experiments disagreeing mutually, whether in determining the critical Rayleigh number (Figure 1.2) or in determining the heat transfer efficiency at very high Rayleigh numbers (Figure 1.6). Because of the big importance for many scientific areas like astrophysics, geophysics and technological applications, there is great motivation to study this phenomenon and to figure out these differences.

The effect of thermal radiation at room temperatures on natural convection have been widely studied in previous years, for example the side-wall radiation and effect of radiation on onset of convection [30, 36, 40]. On the first look, the thermal radiative contribution to the convective heat transport in RBC seems to be negligibly small at cryogenic temperatures, according to Stefan-Boltzmann law. However, there is a strong enhancement of radiative heat transfer between two surfaces due to the thermal near field (NF) which can span over a few millimeters at low temperatures (see table 1.2). The heat transferred between two objects by NF can exceed the amount of heat transfer between two black bodies at the same temperatures by more than one hundred times [15].

The onset of convection with cryogenic helium is usually studied in the experimental cell where heating and cooling plates are very close to each other (1 mm and less [13,18]). This is because the Rayleigh number depends on the cube of distance and the onset of convection occurs at relatively small Rayleigh numbers. On the small distance between the plates, NF from one plate can reach the opposite surface and affect the experiment.

Thermal boundary layers (BLs) inside the RBC system, adjacent to the top and bottom plates of the cryogenic experimental cell, can have also small thiknesses (below 1 mm), especially at high Rayleigh numbers (see Figure 2.5). The temperature sensors have to be put really nearby the heating and cooling plates to study temperature profile and thermal fluctuations of the BLs. Sensors usually used at cryogenic temperatures are very sensitive and even a small amount of heat can affect their measurements.

When we don't know about the effects affecting the temperature sensors in our experiment, it can cause many problems. These can be good reasons for thinking about the NF effect on cryogenic RBC studies. Furthermore, one can speculate whether some amount of heat by NF can be transferred through the BLs directly into the turbulent core of RBC (by means of still unknown mechanism) and affects thus studied dependences on the heat transfer efficiency in RBC.

3

In cryogenic RBC experiments, the cooling and heating plates in the upper and lower part of the experimental cell are mostly made of copper because of their high thermal conductivity at cryogenic temperatures. Measurements of the thermal radiation even with its near field part for Cu plates haven't been done before and its influence on RBC experiments wasn't calculated too. These are the reasons why the Cu was chosen to study its radiative power from the NF, as well as the motivation for our work on the current thesis.

The thesis is organized as follows. Chapter 1 introduces the theoretical foundation of the RBC and NF. Dimensionless numbers describing the RBC are defined and a basic description of the heat transfer efficiency by $Nu(Ra, Pr)$ scalings are presented there. Next, few ways of finding the onset of convection in RBC are outlined and simple temperature profile is described. Then, NF is presented together with an apparatus used for the measurements of NF. In chapter 2, the preparation of the Cu samples for the measurements of NF and the process of the measurements are described. Data from the measurements are presented here too. Then, these data are used for evaluation of the effect of NF on the onset of convection and on measurements with two types of small commercial temperature sensors. In the last part, the comparison of the radiative heat transfer at the distances given by the thickness of boundary layers with the convective heat transfer is done for three cryogenic experiments. Chapter 3 summarizes the results and the conclusions of the thesis.

1. Theory

1.1. Rayleigh-Bénard convection

The Rayleigh-Bénard Convection (RBC) is a physical model for study of fluid flows by natural convection between two parallel horizontal plates mutually displaced by distance L in the gravitational field. The flow is generated by the differing temperatures between the hotter bottom plate T_b and the colder top plate T_t. Within the Oberbeck-Boussinesq approximation [4] (this means, all fluid properties are assumed to be constant except for linearly temperature-dependent density in the buoyancy term) the dynamics of RBC is described by the two dimensionless control parameters, namely, the Rayleigh number Ra and the Prandtl number Pr,

$$Ra = \frac{g\alpha\Delta T L^3}{\nu\kappa}, \qquad Pr = \frac{\nu}{\kappa} \tag{1.1}$$

where g stands for the gravitational acceleration; $\Delta T = T_b - T_t$, is the temperature difference between the bottom and the top plate. The working fluid is characterized by the combination $\alpha/\nu\kappa$, where α is the isobaric thermal expansion, ν is the kinematic viscosity, and κ denotes the thermal diffusivity.

The Ra number represents the ratio between thermally induced buoyancy and the viscous and thermal diffusive effects. The Pr number describes the thermophysical properties of the working fluid.

In a laboratory, the RBC is usually realized in a cylindrical convection cell with adiabatic sidewall. The geometry of the cell is characterized by the aspect ratio Γ

$$\Gamma = \frac{D}{L} \tag{1.2}$$

where D is the diameter and L is the height of the cell.

Table 1.1 contains some examples of turbulent natural convection systems with corresponding estimates of orders of magnitude of Ra and Pr numbers and vertical scales represented by height L with aspect ratio Γ. We can notice that all parameters vary in a wide range. This wide range is a great challenge for theoretical and numerical modeling of RBC and for laboratory experiments to cover. Yet, the cryogenic laboratory experiments seem most capable of approaching the desired ranges of Ra [27].

Table 1.1: Examples of natural convection systems with estimates of their main characteristics [10]: the Rayleigh (Ra) and Prandtl (Pr) dimensionless numbers, the typical vertical scales L and the aspect ratios $\Gamma = D/L$.

	Ra	Pr	L	Γ
Processor cooling device	10^6	0.7	1-10 cm	1
Indoor ventilation	$10^8 - 10^{10}$	0.7	1-10 m	1-10
Deep oceanic convection	$10^{23} - 10^{27}$	7	1-4 km	$10^2 - 10^3$
Mantle convection	$10^7 - 10^9$	10^{23}	700 km	54
Solar convection zone	$10^{20} - 10^{24}$	$10^{-7} - 10^{-3}$	$2 \cdot 10^5$ km	10

Onset of convection (a buoyancy-driven instability) is characterized by the critical Rayleigh number Ra_c. At this value, the stability of the fluid layer is broken and the convection begins to play a big role in an efficiency of the heat transfer and mass flow, surpassing gradually the heat transfer by conduction. Theoretically predicted value is $Ra_c = 1708$ for $\Gamma = \infty$ [7]. This value Ra_c increases for aspect ratio $\Gamma < 10$ [8].

When fluid starts to flow inside the cell, hot less dense fluid rises and cold denser fluid falls in some regions. This process of rising and falling of the fluid can be formed to flow patterns. The simplest example of such pattern of convective flow for aspect ratio $\Gamma \geq 1$ is straight, counter-rotating parallel rolls shown in Figure 1.1. Hexagons or squares could be formed by the superposition of rolls [11].
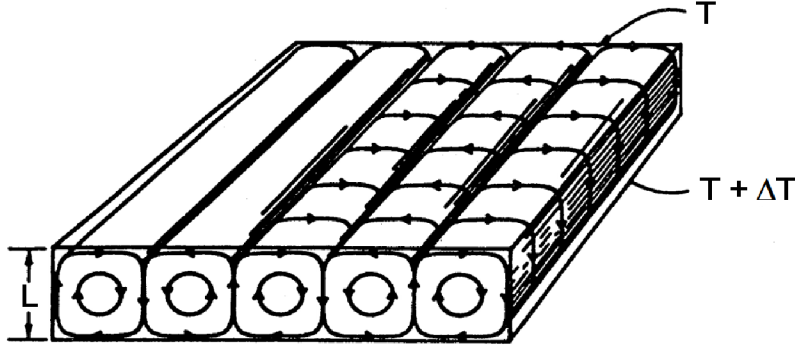
Figure 1.1: Roll flow pattern in Rayleigh-Bénard convection [11]

The efficiency of the convective heat transfer is described by the Nusselt number Nu,

$$Nu = \frac{Q_t}{Q_\lambda} \tag{1.3}$$

which is the ratio of the total heat flow Q_t through the RBC system reduced by the heat flow Q_λ that would be transferred by conduction only. The Nusselt number Nu is not control parameter like Ra or Pr, but it's called response parameter. For condition where $Ra < Ra_c$ there is no convection and $Nu = 1$. It is known as a conduction regime.

The conductive heat flow Q_λ can be calculated by the equation,

$$Q_\lambda = \lambda \frac{S}{L} \Delta T, \tag{1.4}$$

where λ is the thermal conductivity and S is an area of the plates. When $Ra > Ra_c$ convection occurs and thus $Nu > 1$.

For any given set of Ra and Pr control parameters in the RBC system, the dimensionless heat transfer is expressed in terms of the Nusselt number, Nu. Figure 1.2 shows some dependences of Nu on Ra number reduced by critical Rayleigh number Ra_c near the onset of convection for different aspect ratios Γ. Further behavior of Nu is the target of many theoretical, numerical and experimental studies around the world [2,9,26,38,39].
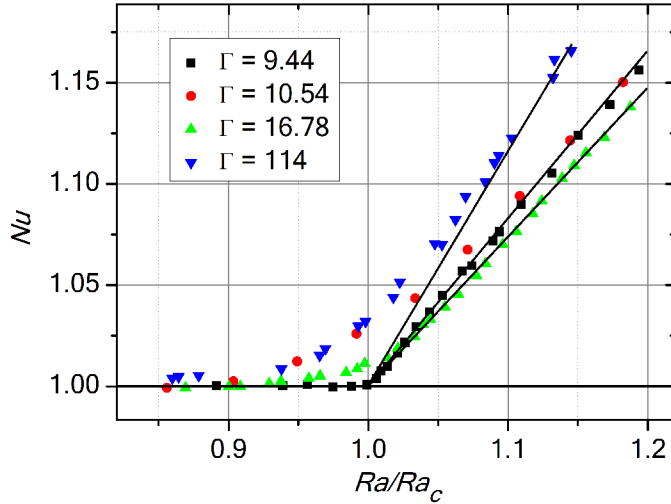
Figure 1.2: Measurements of Nusselt number Nu versus Rayleigh number Ra reduced by the critical Rayleigh number Ra_c for different aspect ratios measured by different scientific groups. These measurements can be used to determine the onset of convection. All measurements were done at cryogenic temperatures [13].

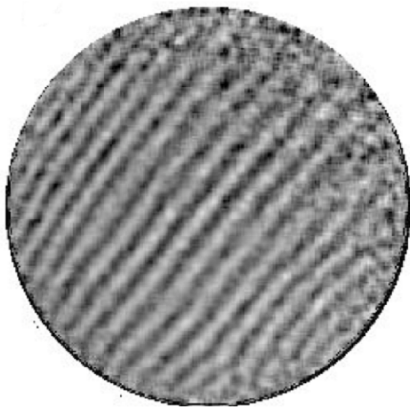### 1.1.1. Onset of convection - critical Rayleigh number determination

Mostly used way to find the onset of convection is from Nu (see eq. 1.3). When convection occurs, Nusselt number Nu will increase as is shown in Figure 1.2. This can be seen when we plot the temperature difference ΔT between the plates on a heat power applied to the bottom plate Q_b. The ΔT is linear to this applied heat power Q_b in conduction regime. This linear relationship is shown in equation 1.4. After the onset of convection, as ΔT increases and past a critical value (determining the critical number Ra_c), there is a drop in the ΔT because the heat is transported by convection more effectively. It is shown in Figure 1.3.
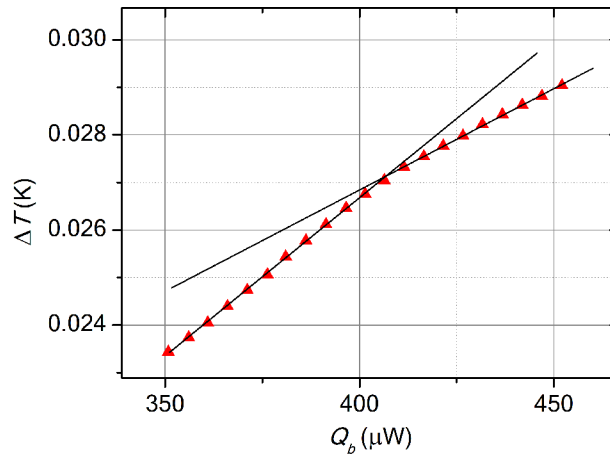

Figure 1.3: One method how to find the onset of convection: dependence of the tempereture difference ΔT betwen the plates on the heat power Q_b applied to the bottom plate. Linear dependence of ΔT on Q_b is broken when convection occurs. Adapted from [20]

7

Another way how to find the onset of convection is by using optical visualization techniques. We know that when convection occurs, the stability is broken. This would be seen as the flow of the fluid and as the formation of flow patterns. To visualize the flow pattern of the fluid, a shadowgraphy method can be used [20]. In the shadowgraphy method, the light passes through the fluid and leave it with different phase. This is caused by a various refractive index corresponding to various temperatures and densities. After the process where different phases of the light are transformed into intensity distribution [20]. The example of the roll flow pattern above the onset of convection obtained by shadowgraphy method in the cryogenic experiment [19] is shown on the left-hand side of Figure 1.4 where the top view is captured. On the right-hand side, there is a numerical simulation of the same flow pattern.

However, it is difficult to determine the critical Ra_c (the critical temperature difference ΔT) from a visual point of view. We cannot say that the onset of convection is only present when we see the rolls. This is the reason why the use of the Nusselt number Nu is preferred.

(a) Visualization of the flow pattern with shadowgraph
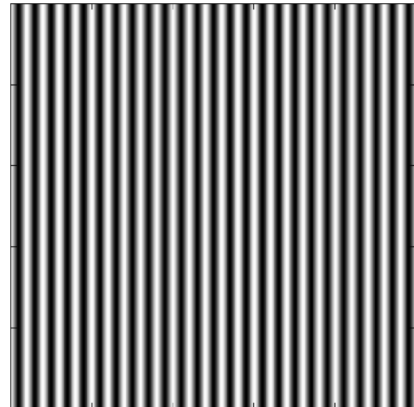
(b) Numerical simulation of straight roll pattern

Figure 1.4: (a) Top-view shadowgraphy picture of straight roll pattern above the onset of convection at Rayleigh number $Ra = 2766$, Prandtl number $Pr = 0.496$ and aspect ratio $\Gamma = 33.2$ [19]. (b) Numerical simulation of straight roll pattern at Rayleigh number $Ra = 2647$, Prandtl number $Pr = 1$ and aspect ratio $\Gamma = 100$. Only part of the numerical simulation is visible [32].

Actually, some experiments with helium at cryogenic temperatures have shown uncertaintees in finding the onset of convection [8, 18]. Big inaccuracy is because of imperfect knowledge of fluid parameters. It can make 20% of combined uncertainty in Ra_c from α, ν and κ. The Figure 1.2 shows dependences of Nu on Ra/Ra_c in four experiments for different aspect ratios Γ. For high aspect ratio Γ, the critical Rayleigh number Ra_c is supposed to converge to value $Ra_c = 1708$ but in Figure 1.2, Ra_c is getting lower.

Another experiment, where big uncertainty occurs in finding Ra_c, was done by Matthew J. Lees et al. [18]. Aspect ratio Γ of their experimental cell is 33.2. They got a value $Ra_c = 1857$ at mid-plane temperature $T = 2.209\,\text{K}$ and with increasing temperature they observed incresing Ra_c up to value $Ra_c = 2443$ at mid-plane temperature $T = 3.077\,\text{K}$. These values lie above the theoretical value $Ra_c = 1708$. This is in contrast with experiments in Figure 1.2.

1.1.2. Temperature profiles

For a complete understanding of RBC, knowledge of a temperature profile is really important. In the conduction state, the temperature profile is linear throughout the whole height L of the cell. It is visualized in Figure 1.5 by a green dash-dot line. When we study the temperature profile of convecting fluid inside the cell, we would observe that nearly whole temperature difference ΔT is accomplished by two thermal boundary layers (BLs) closed to the top and bottom plate. The rest of the interior is nearly isothermal with temperature fluctuations. Approximately $\frac{\Delta T}{2}$ is in the top BL and another $\frac{\Delta T}{2}$ is in the bottom BL for the Oberbeck-Boussinesq RBC [1] as is shown schematically in Figure 1.5.
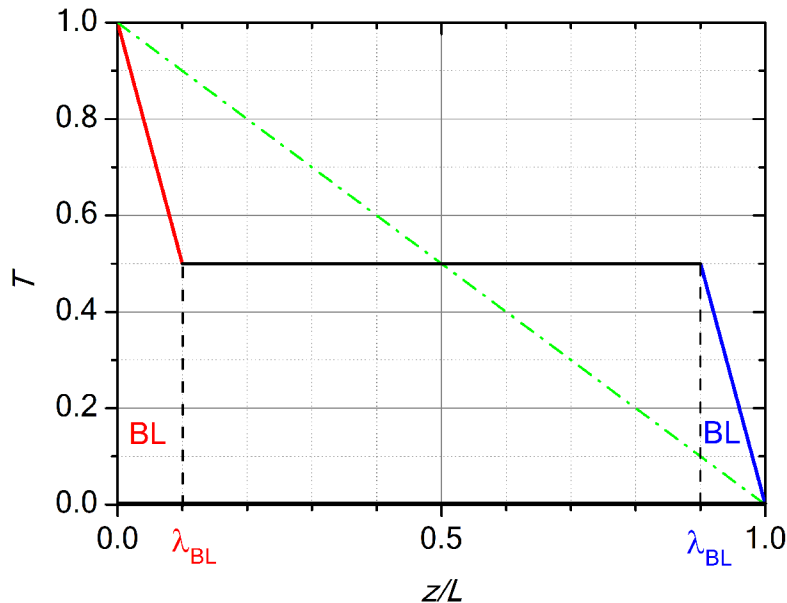
Figure 1.5: A schematic diagram of temperature profile in conduction state (green dash-dot line) and in convection state (thick line). T represents normalized vertical temperature, z/L is normalized vertical distance where $z = 0$ is the position of the bottom plate [12].

The thickness of thermal BLs can be calculated [38] as

$$\lambda_{BL} = \frac{L}{2Nu} \tag{1.5}$$

However, for higher Ra, non-Oberbeck–Boussinesq effects can cause some asymmetries in thicknesses of BL [38]. To study these BLs, we have to put the temperature sensors really nearby the plates of the chamber and there is given a big emphasis on precision of sensors. These issues are discussed in section 2.3.

1.1.3. The heat transfer efficiency at high Rayleigh numbers – controversy in cryogenic experiments

The functional dependence $Nu\,(Ra, Pr)$ is usually expressed as a scaling law $\propto Ra^{\gamma}Pr^{\beta}$. The RBC fluid layer becomes turbulent typically at Rayleigh numbers Ra exceeding 10^5, except for the boundary layers. A value of the power exponent γ close

to 1/3 is obtained from theories and various laboratory experiments or numerical simulations for turbulent RBC (for review see [2]). Two independent theories of Castaing [6] and Shraiman and Siggia [33] for turbulent RBC resulted in $\gamma = 2/7$, whilst Malkus [23] derived $\gamma = 1/3$. These theories predict either a relatively weak or none at all dependence on Pr [2]. For the power exponent $\gamma = 1/3$, the transferred heat does not depend on the height L. This property is consistent with a simple model of convection where all the temperature difference ΔT is on the BLs (thin in comparison with L) while the central fluid is effectively mixed due to the turbulence and has nearly constant temperature T_m. The heat transfer is thus controlled by the heat conduction of the thermal BLs which become thinner with increasing heat flux (see Eq. 1.5).

On the other hand, the ultimate regime of RBC with turbulent boundary layers was predicted by Kraichnan in 1962 [14]. In this regime, the heat is transferred much more effectively and Nu should scale with Ra with power exponent $\gamma = 1/2$. The existence of the ultimate regime is one of the most discussed topics in the field of RBC. Confirmation of such a regime would be of great importance for understanding many natural and practical phenomena, as the heat transport efficiency rises significantly.

The experimental dependences of $Nu(Ra)$ observed in three independent cryogenic experiments [26, 31, 39] for similar aspect ratio $\Gamma \approx 1$ are shown in Figure 1.6 [38]. After applying side-walls correction on parasitic heat flow [38], all of them follow the same scaling $Nu \propto Ra^{2/7}$ at the left-hand side of the graph. At higher Ra, the data differ significantly. Brno data follow the $Nu(Ra)$ dependence with the value of coefficient $\gamma = 1/3$ predicted by Malkus [23]. On the opposite, the Grenoble and Trieste data follows the steeper dependences with a higher value of γ. While the Grenoble group observed the transition to the scaling law with higher power exponent $\gamma \sim 0.4$ interpreted as the transition to the ultimate regime, Trieste group found a scaling law with γ exponent slightly higher than 1/3.
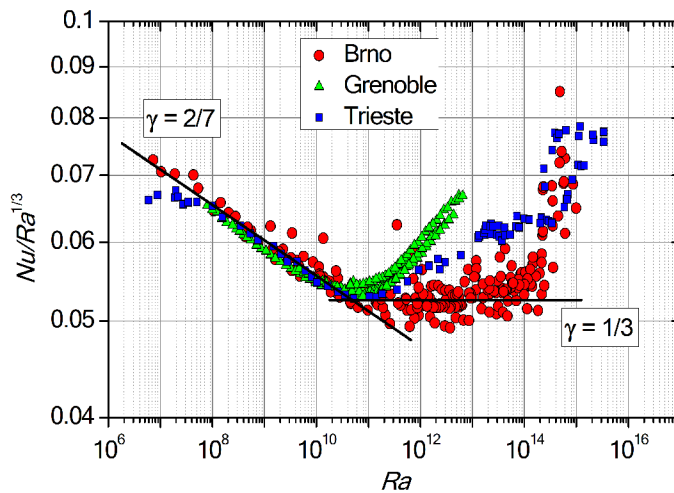
Figure 1.6: The reduced $Nu/Ra^{1/3}$ plot versus Ra where experimental data of Nu are by three different experimental groups. On the left hand side, all the data follow the same dependence $Nu \propto Ra^{2/7}$ after side-wall corrections [39]. On the right hand side, only the data from Brno follow dependence $Nu \propto Ra^{1/3}$ predicted by Malkus [23]. Why the dependences differ at high Ra is still being discussed.

It is still being discussed why the values of coefficient γ differ on the right-hand side of Figure 1.6. A possible explanation is that it is due to the non-Oberbeck–Boussinesq effects which can play a big role there [34, 37, 38].

1.2. Thermal radiative Near field

1.2.1. Basic equations for radiative heat transfer

Every object emits electromagnetic radiation - thermal radiation. Principially maximal amount of energy radiated from a body is described by the Stefan-Boltzmann law which is integral of the Planck's law.

$$Q_{BB} = \sigma S T^4 \tag{1.6}$$

where σ is Stefan–Boltzmann constant, S is the area of the surface and T is temperature of the body. This radiation is called Black body radiation and surface radiating a maximum of the thermal radiation we call black surface.

Maximum heat transfer between two infinite plane parallel black surfaces at different temperatures is then given by the difference of the radiative heat flows

$$Q_{BB} = \sigma S(T_2^4 - T_1^4) \tag{1.7}$$

where T_1 is temperature of the cold object and T_2 is temperature of the hot object.

A real surface will emit or absorb a smaller amount of the thermal radiation than it is defined by the Stefan Boltzmann law. The effectiveness in emitting of the thermal radiation is the emissivity of the surface. The emissivity is the ratio of the thermal radiation from a surface to the radiation from the black surface at the same temperature and of the same area. Similarly, we can define absorptivity as the ratio of the heat flux absorbed by a real surface to the heat flux absorbed by the Black body at the same conditions.

The Stefan-Boltzmann law assumes that the heat exchange is done over distances larger than the wavelengths of the radiation. The radiative heat transfer between plane parallel surfaces is then independent on the distance L between them. In that case, we speak about far field radiation (FF).

However, when two surfaces are really close to each other the heat flux increases. Its value can exceed the value of heat flux given by Black body radiation more than a hundred times [15]. It's because, in parallel with the thermal radiation, there are the evanescent waves propagating along the surface of the material. Their energy decreases exponentially with the distance d from the surface. When the field of evanescent waves reaches the opposite surface, the energy can be transferred by tunneling of photons. This evanescent field is also called near field (NF). The distance d where the NF becomes dominant can be calculated by [28]

$$d < \lambda_{BB} = \frac{c_0 \hbar}{k_B T} \tag{1.8}$$

where λ_{BB} is characteristic wavelength of the Black body radiation at temperature T, c_0 is the velocity of light in free space, $\hbar$ is reduced Planck's constant and k_B is Boltzmann's constant. Some calculated values with this equation are in table 1.2. We can see that for cryogenic temperatures it can span over a few millimeters.

Table 1.2: Distances (characteristic wavelength), where the near field starts to be dominant over the far field for different temperatures, calculated with equation 1.8 [28].

| T (K)	λ_{BB} (μm)
1	2289.8
4.2	545.2
100	22.9
273	8.4
1000	2.3

The sources of NF and FF are fluctuating currents given by fluctuation dissipation theorem [22, 29]. This source can be put into the Maxwell equations. With the use of Green's function formalism, we can get a solution for the electromagnetic field, heat transfer and force interaction. But theoretical calculations aren't part of this study. Instead of theoretical calculations, direct measurements of the dependence of the heat flux between the surfaces are done with an apparatus described in the next section.

1.2.2. Evanescent wave apparatus

The evanescent wave apparatus (EWA), in Figure 1.7, used for the measurement of the radiative heat transfer between two circular plates (samples) with different temperatures in vacuum was designed and assembled at the Institute of Scientific Instruments in Brno by T. Králík et al. [16]. A hotter sample with the temperature T_2 acts as the emitter and a colder sample with temperature T_1 is absorber. Measuring the heat transfer over the gap between the samples which can be adjusted from $1\,\mu$m to about $500\,\mu$m which allows us to study FF, NF and transition from FF to NF. EWA operates at cryogenic temperatures. Cryogenic temperatures offer the advantage of the longer range of the NF (tens of μm), excellent vacuum condition (10^{-8} Pa), low parasitic thermal radiation and very sensitive thermometry (10-50 μK).

Apparatus EWA is 100 cm long and has 48 mm in diameter. Almost the whole apparatus has to be put in a wide neck LHe dewar before the measurement. Only a lid with a valve for the evacuation of the apparatus, the electrical feedthrough, a knob to set up the gap between the samples and an electric capacitance meter below the lid are above the Dewar not sunk in the LHe. In the upper section of a part sunk in the Dewar are radiation shield (RS) disks mediating connection with LHe bath, working as a shield against radiation propagating from the lid. Another role of the RS disks is to prevent the vacuum jacket to collapse after the evacuation and cooling down of the apparatus. They are shown in Figure 1.7b.

A knob with a scale with 2° resolution at the lid is used to turn the shaft going through a holder tube to a differential screw. The holder tube connects the lid and a
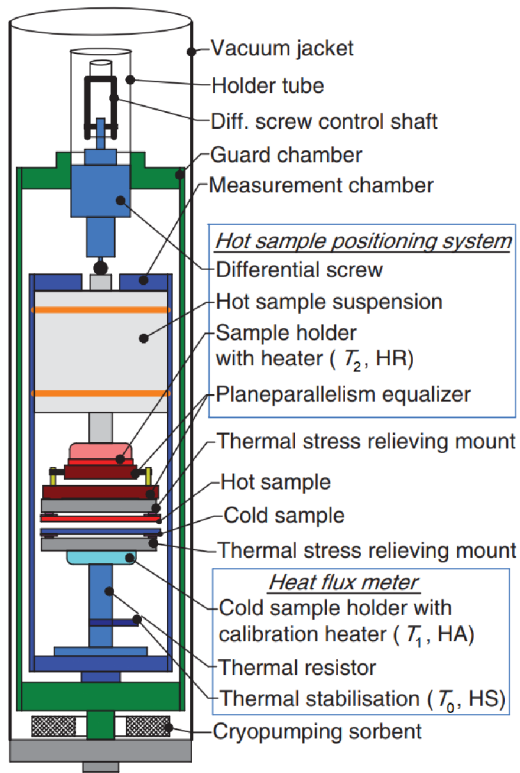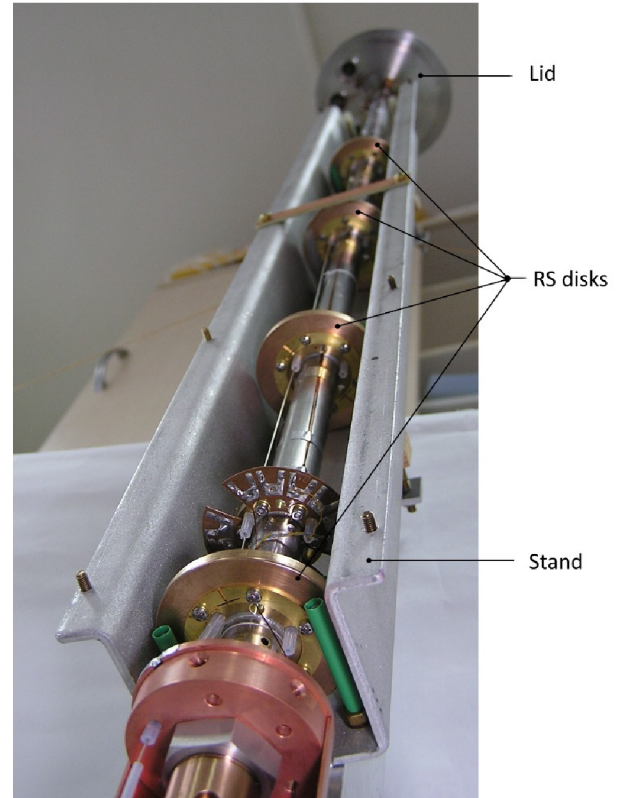
**(a)**   **(b)**

Figure 1.7: (a): Scheme of the lower part of the apparatus. (b): The upper part of the apparatus.

guard chamber (Figure 1.7a) which protects a measurement chamber against mechanical stress and heat flow coming from the holder tube. The differential screw has a pitch of $100\,\mu$m per revolution. This differential screw acts on a hot sample suspension. The hot sample suspension based on metallic membranes is there to minimize instabilities in axial motion due to friction and backlash [16].

Under the hot sample suspension, there is a sample holder with a heater connected to the planeparallelism equalizer which is based on three friction locks each made of a pair of perpendicular pins. To set the samples plane parallel, we first have to go down with the upper sample to achieve contact with the lower sample. The contact is detected by means of capacitance meter. Due to direct contact between them, they become plane parallel. The friction locks of the planeparallelism equalizer will then keep the hot sample in the same position when going up with it.

Both samples are attached to thermal stress relieving mount which is there to decrease mechanical stress due to thermal contraction mismatch between the samples and their holders (Figure 1.7a. The cold sample holder is a part of a heat flux meter (HFM) composed of a calibration heater, a thermal resistor made of a thin-wall stainless steel tube, stabilization heater, and two temperature sensors (see Figure 1.8). One sensor is mounted to the cold sample holder together with the heater used for HFM calibration. The second one is at 1/5 of the thermal resistor height together with the stabilization heater. The lower end of the thermal resistor is soldered to a copper flange. This flange

13
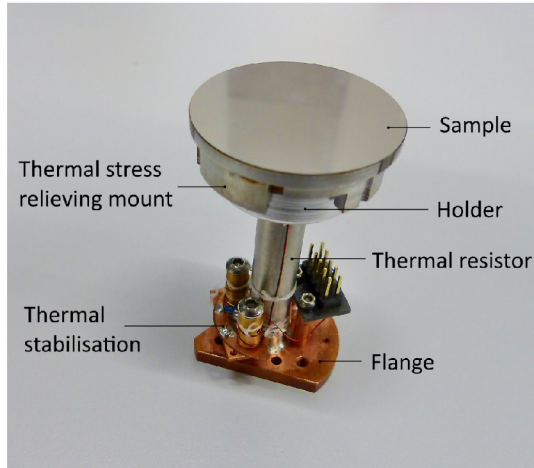
Figure 1.8: Heat flux meter with Nb sample. The Cu sample was used in our study.

is bolted to the bottom of the measurement chamber and thus it is thermally connected to the LHe bath.

The measurement chamber is made of 1 mm thick copper coated by an epoxy layer laminate at the inner surface to reduce reflection of the thermal radiation. The whole apparatus is housed in a vacuum jacket. During the evacuation, we can reach $\sim 10^{-2}$ Pa at room temperature. Because of using charcoal sorbent at the bottom of the apparatus we can reach the pressure $\sim 10^{-8}$ Pa by adsorption when cooling down at LHe temperature.

The size of the gap between the samples can be read on the adjustment knob of the differential screw or by direct measurement of the electric capacitance between the samples. The sample layers serve as electrodes. The hot sample is connected with the capacitance meter and the cold sample is connected to the electrical earth of the apparatus.

2. Measurements and results

2.1. Measurement of the radiative heat transfer between copper samples

In the beginning, we had to do some service of the apparatus because of the long inactive period. This includes treatment of almost all rubber o-rings used as the sealings with silicone vacuum grease and the RS disks (Figure 1.7b) with Apiezon N grease. To put samples in, it is needed to pull the whole inner part from the vacuum jacket, open the guard chamber and open the measurement chamber. Then we have to take out heat flux meter out of the chamber. This part is in Figure 1.8.

A sputtered film of Cu on a sapphire substrate was used as the sample. The sapphire substrate was chosen because of its high thermal conductivity and dimensional stability. Cu was chosen because this material is mostly used in RBC experiments. The substrate disk has 35 mm in diameter and is 2.7 mm thick. The Cu film has 720 nm in thickness. The Cu film can't be too thin, because then it could be transparent for long wavelengths of the thermal radiation.

To attach the samples, three sample pads are glued with epoxy HYSOL® 9481™ (Loctite) on the samples. With these pads, each sample can be attached to the thermal stress relieving mount. When this is done, cryogenic coaxial cable for the capacitance measurement of the distance between the samples is soldered to the hot sample. After this, the measurement chamber together with guard chamber can be closed and the whole apparatus can be put into the vacuum jacket again. This operation is done in clean room conditions in the laboratory of the electron lithography to prevent sample surfaces against dust particles.

After this, the evacuation at room temperature can happen and then apparatus is inserted in the LHe Dewar after precooling in LN_2.

Before the measurement, the plane parallelism is set up in the way it was described above in the apparatus section. With this, we can already configure our parameters of the experiment. There are two ways of doing it. The first way is to keep the constant gap d between the samples and changing temperature of the hot sample T_2. The results can be seen in Figure 2.1a. The second way is to keep the constant temperature of the hot sample T_2 and to change the distance d. Data from these measurements are in Figure 2.1b. All values in both plots are shown as the specific heat flux Q_R/S, where Q_R is radiative heat flow between the samples and S is the sample area. Q_R is measured with the heat flow meter (HFM).

The heat flow Q_R, which is absorbed by the colder sample, is evaluated from the calibration curve of HFM which is represented by the dependence of heat flow Q_{HA} supplied by a calibration heater on the temperature difference $T_1 - T_0$ where T_1 is the temperature of the absorber (cold sample) after it gets to equilibrium and T_0 is temperature of thermal stabilisation.

The HFM is calibrated using an electrical heater. The temperature of the thermal stabilization T_0 is always kept at 5 K. The resolution of the thermometers is important for the calibration procedure and the evaluation of the Q_R from the calibration curve $Q_{HA}(T_1 - T_2)$. Their reproducibility, uncertainty in the calibrating electrical power, and
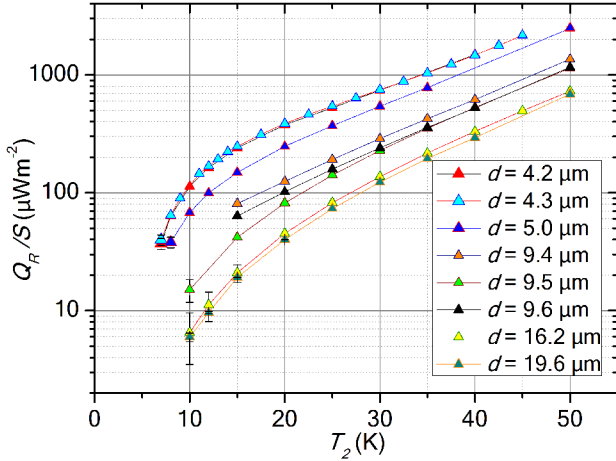
(a) Measurement with the constant distance d
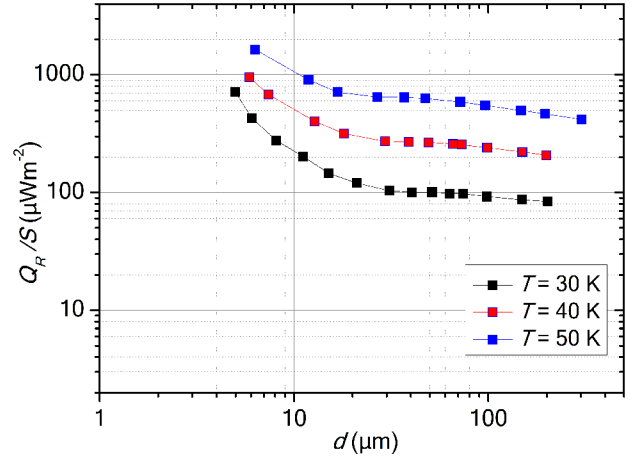
(b) Measurement with the constant temperature T_2

Figure 2.1: Values of specific heat flux Q_R/S where Q_R is radiative heat flow measured with the heat flow meter on the EWA. S is the area of the samples. (a) is measured when the constant distance was kept and (b) is for constant temperature. The error bars are plotted only for uncertainties bigger than 10%.

the electrical stability are the additional effects which contribute to the uncertainty of the Q_R measurements [25].

The temperatures of cold sample T_1, hot sample T_2 and thermal stabilization T_0 are measured by Cernox® CX 1050 SD sensor with low power dissipation $0.4\,\mu W$. The temperatures are monitored and controlled by temperature controller LakeShore 340. Resolutions of the temperature measurements are $T_{0,1,res} = 50\,\mu K$ for $T < 10\,K$ and $500\,\mu K$ for $T > 10\,K$.

To minimize the noise caused by external electromagnetic fields, inductor-capacitor (LC) filters are on the cables supplying the apparatus with electricity. But still, there would be some parasitic heating (sensor self-heating) inside the chamber. We can minimize this effect by measuring it at the beginning as a background and then easily subtract it from the measured heat flow Q_R.

The total uncertainty of the measured heat flow Q_R can be written as [25]

$$\delta Q_R < 3.8 T_1^{1.222}(T_{1,res} + T_{0,res}) + (b+c)Q_R. \tag{2.1}$$

Coefficient b is contribution due to the unstable background and for the calculations has a value $b = 0.01$. Coefficient c has a value $c = 0,02$ and it is due to uncertainty in the calibration curve [25]. In all graphs, the error bars are marked only at values with uncertainty bigger then 10%. There are some selected uncertainties in table 2.1.

One set of measurements (one curve in Figures 2.1, 2.2, 2.3) is usually done in 6-8 hours. Every time, we wait at least 20 minutes for a steady state before we write down another value. The heat flow gained from the measurements is the mean value from the last two minutes to minimize the influence of the temperature fluctuations and noise of the sensors.

Table 2.1: Examples of radiative heat flows Q_R and temperatures of the absorber T_1 measured in the apparatus EWA together with absolute and relative uncertainties of QR calculated using Eq. 2.1

T_1 (K)	Q_R (μW)	δQ_R (μW)	δQ_R (%)
5.0322	0.6849	0.02329	3.40
5.0010	0.0403	0.00393	9.74
5.0006	0.0184	0.00327	17.75
5.0003	0.0093	0.00299	32.33
5.0002	0.0057	0.00289	50.37

For further data analysis, it's practical to express the results Q_R reduced by the heat flow between black surfaces using Eq. 1.7. Let's call it coefficient of the radiative heat transfer

$$\varepsilon\,(T,d) = \frac{Q_R}{Q_{BB}} = \frac{Q_R}{\sigma S(T_2^4 - T_1^4)} \tag{2.2}$$

where Q_R is measured heat flow. You can see results in Figure 2.2a, 2.2b. But still it is really hard to fit there some model. In that case another improvement has to be done. By using hot sample temperature T_2 multiplied by distance between the samples d as a variable, the results will nearly collapse into one curve. This is shown in Figure 2.3.
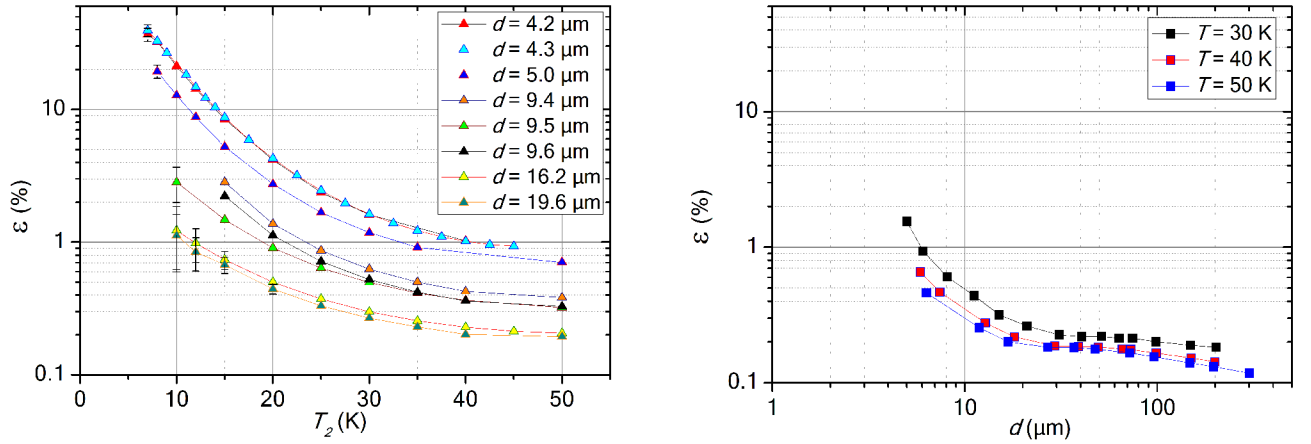
(a) Measurement with the constant distance d

(b) Measurement with the constant temperature T_2

Figure 2.2: Values of the coefficients of the radiative heat transfer ε (see Eq. 2.2) for two ways of measurements where the constant distance d or constant temperature T_2 is kept. The error bars are plotted only for uncertainties bigger than 10%.

Now, it is possible to fit the data with the following model.

$$\varepsilon = a_0 + a_1(Td)^{a_2} + \frac{a_3}{Td^{a_4}} \tag{2.3}$$

where a_n are the parameters we have to find. Here, a_0, a_1 and a_2 characterise FF contribution while a_3 and a_4 are for NF. For the calculation, the least squares method was used. FF and NF were fitted separately because even a small deviation in NF has a more
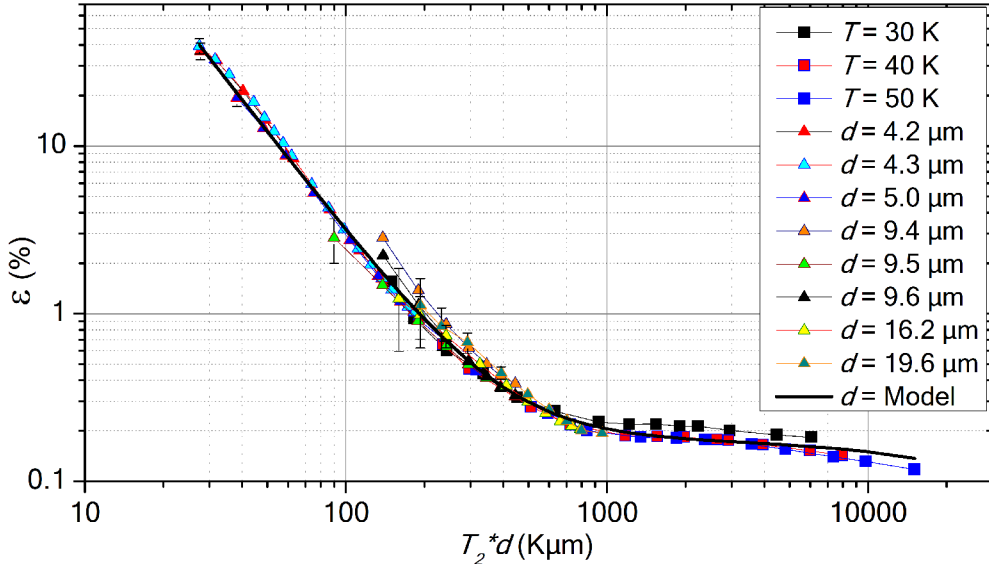
Figure 2.3: All results of the coefficients of the radiative heat transfer ε obtained from equation 2.2. The results from both ways of measurements (with constant d or T_2) collapse into one dependence when the product of distance d and temperature T_2 is used. The data in this plot can be fitted (black line) by equation 2.3 with coefficients in table 2.2. The error bars are plotted only for uncertainties bigger than 10%.

significant influence on the sum of squares than in the FF. Values of coefficients are in tab. 2.2. In Figure 2.3, the model is shown as a black line.

Table 2.2: Coefficients in eq. 2.3 found with use of least square method.

a_0	a_1 $(\mathrm{K}^{-a_2}\mu\mathrm{m}^{-a_2})$	a_2	a_3 $(\mathrm{K}^{a_4}\mu\mathrm{m}^{a_4})$	a_4
0.167	$-1.67 \cdot 10^{-11}$	2.14	$2.16 \cdot 10^4$	1.9

2.2. The effect of NF on onset of convection

Here we will focus on the experiment done by Matthew J. Lees et al. [18]. These measurements were done in a cylindrical cell with aspect ratio $\Gamma = 33.2$. The diameter is $D = 18.26\,\mathrm{mm}$ and height is $L = 0.55\,\mathrm{mm}$. The cell contains liquid helium. The mid-plane temperature of LHe varied in the range from $2.2\,\mathrm{K}$ to $3.1\,\mathrm{K}$. When they measured the Ra_c, they got values close to 1800 at $2.2\,\mathrm{K}$. With increasing temperature, they observed rising Ra_c up to around 2500 at the highest temperature $T_m = 3.1\,\mathrm{K}$. This is significantly above the theoretical value $Ra_c = 1708$ [18].

They used Cu for the hot bottom plate and sapphire for the cold top one. The transparent top plate allows to visualize the flow pattern above the onset of convection [20]. To find the onset of convection, they used the method of the dependence of ΔT on applied heat power to the bottom plate (see sec. 1.1.1) and shadowgraph method.

Their measured values Ra_c and parameters of the experiments are shown in the tab. 2.3. Reasons, why we focus on this experiment, are the height of the cell and working temperature. When we compare them with the values in the tab. 1.2 or with the eq. 1.8, there is a possibility of the near field influence on transferred heat.

Table 2.3: Properties of the fluid, temperature difference between the plates ΔT and critical Rayleigh numbers Ra_c for mid-plane temperatures T_m for the experiment by Lees et al. [18]

T_m (K)	ΔT (K)	α (1/K)	ν (mm^2/s)	κ (mm^2/s)	Ra_c
2.209	0.0449	0.0127	0.186	0.268	1857
2.233	0.0408	0.0172	0.192	0.299	1992
2.352	0.0389	0.0296	0.212	0.395	2240
2.617	0.0368	0.0445	0.234	0.472	2412
3.077	0.0272	0.0654	0.250	0.476	2443

Calculations are done for Cu plates and the case where one of them is made of sapphire is discussed at the end of this section. Firstly, we have to found the heat transferred in the cell just before the onset of convection. Because the convection is still not there, only conduction is mediating the heat transfer. To calculate the heat flow by conduction Q_λ, we use eq. 1.4. Values of thermal conductivity λ are taken from REFPROP (NIST Reference Fluid Thermodynamic and Transport Properties Database). Results of Q_λ are in the tab. 2.4

Table 2.4: Calculated values of conductive heat flow Q_λ in experiment made by M. Lees [18]. Equation 1.4 was used. Values of thermal conductivity λ are taken from REFPROP database.

T_m (K)	ΔT (K)	λ (mW/m·K)	Q_λ (W)
2.209	0.0449	13.673	$2.923 \cdot 10^{-4}$
2.233	0.0408	13.783	$2.678 \cdot 10^{-4}$
2.352	0.0389	14.302	$2.649 \cdot 10^{-4}$
2.617	0.0368	15.326	$2.685 \cdot 10^{-4}$
3.077	0.0272	16.767	$2.171 \cdot 10^{-4}$

To find how much heat is transferred by radiation, the Stefan-Boltzmann law (eq. 1.7) is used and multiplied by the coefficient of radiative heat transfer which is found in section 2.1

$$Q_R = \varepsilon \sigma S (T_2^4 - T_1^4). \qquad (2.4)$$

The results of radiative heat flow Q_R are summarized in tab. 2.5 and then compared with values of conductive heat flows in Figure 2.4.

Table 2.5: Calculated values of radiative heat flow Q_R for different temperatures in experiment made by M. Lees [18].

T_2 (K)	T_1 (K)	$T \cdot d$ (Kμm)	Q_R (W)
2.231	2.187	1227	$5.60 \cdot 10^{-14}$
2.253	2.213	1239	$5.25 \cdot 10^{-14}$
2.371	2.333	1304	$5.78 \cdot 10^{-14}$
2.635	2.599	1449	$7.38 \cdot 10^{-14}$
3.091	3.063	1700	$8.65 \cdot 10^{-14}$

There is an orders of magnitude difference between the heat transfer by the radiation and by the liquid conduction. When we take into the consideration that one plate was

made of sapphire, the heat transfer should be approximately twice bigger in FF and twice smaller in the NF. Basically, it lowers the differences between far field and near field. On the basis of this analysis, we can conclude that the NF effect do not play any role in determination of the critical Rayleigh number Ra_c in the experiment made by Lees et al. [18].
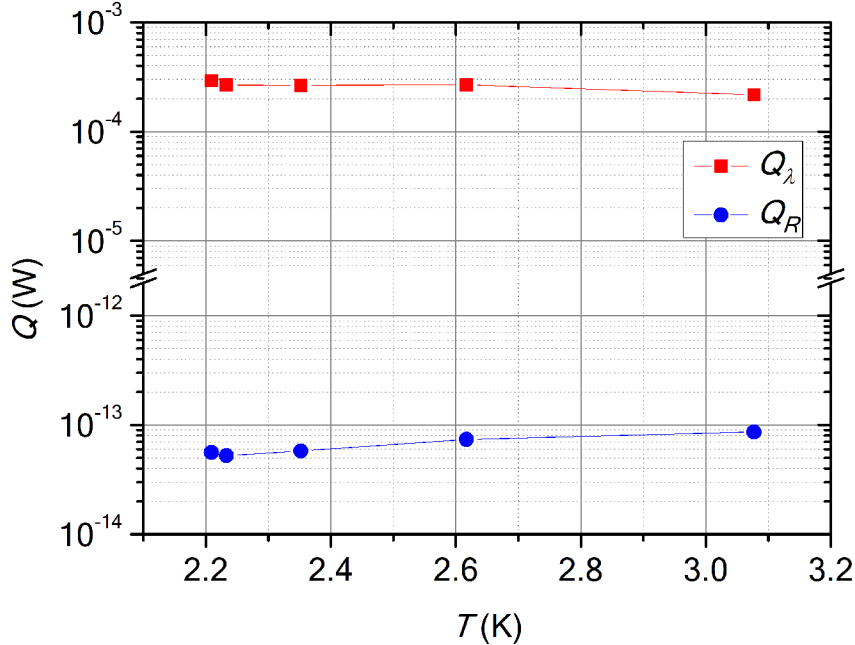

Figure 2.4: Results of conductive heat flow Q_λ (red) and radiative heat flow Q_R (blue). There is ten orders of magnitude difference. Radiative heat flow Q_R is negligible in comparsion with conductive heat flow Q_λ in this experiment made by M. Lees. The thermal near field has no effect on onset of convection in this experiment.

## 2.3. The effect of NF on temperature sensors

In this section, the evaluation of the effect of thermal radiation on temperature sensors is done. Temperature sensors are needed in studying the temperature profiles in cryogenic experiments, especially in the region of thermal BLs. To know which range of distances we are working, the calculations of BL thicknesses has to be done. The data for the calculations of thicknesses of BLs using eq. 1.5 are taken from the experiment accomplished by Urban et al. at ISI in Brno and published in [38,39]. Next to them, there are results by another two scientific groups from Grenoble and Trieste [9,26]. The results are expressed as a dependence of the thermal BLs thickness on Ra in Figure 2.5. You can notice that for higher Ra, the thickness of BL λ_{BL} can reach tens of μm. This prompts us to think about the near field heating of temperature sensors.

When we want to study these BLs, the sensor has to be chosen properly. As small as it can be. Two commercially available sensors, Cernox® and Ge-on-GaAs film resistance thermometer manufactured by companies LakeShore and MicroSensor, respectively, are discussed here.

Cernox® is specifically designed for cryogenic applications and has many advantages, as high sensitivity at low temperatures and good sensitivity over a broad range of tem-
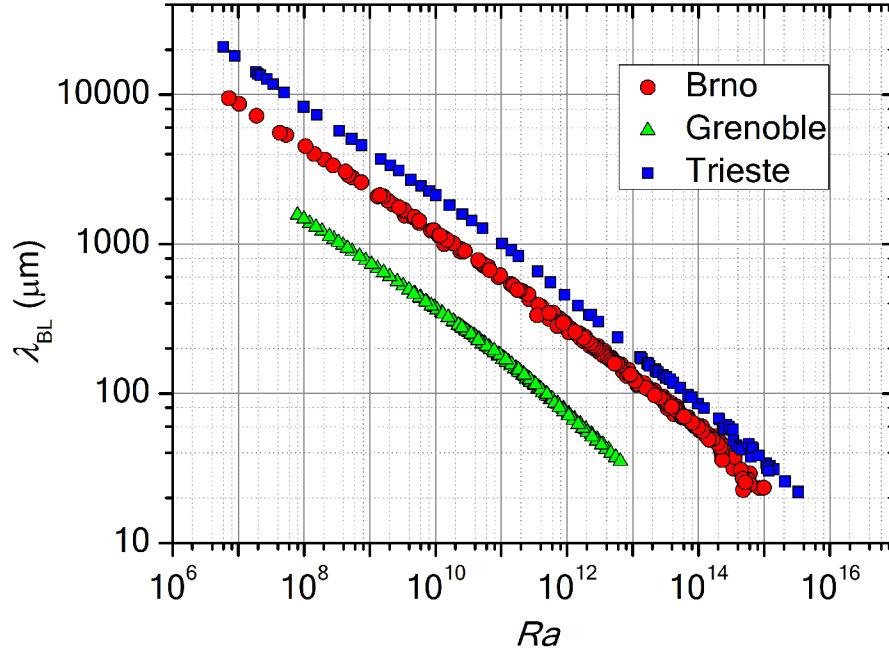
Figure 2.5: Calculated values of thicknesses λ_{BL} of thermal boundary layers in cryogenic experimental cells of aspect ratios $\Gamma \approx 1$ of three different experimental groups.
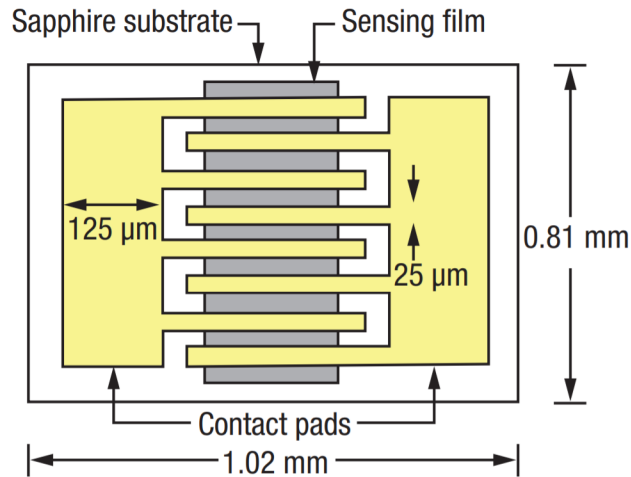

Figure 2.6: Scheme of Cernox® CX-BG sensor by the LakeShore company.

peratures. Cernox® was chosen here because of its small size. You can see a scheme of the sensor in Figure 2.6. It can be used as a bare chip or even with a big variety of packages depending on what we want to use them for. In the study of BLs, small size is required so the bare chip will be used.

Cernox® sheet films are sputtered onto sapphire substrates. Gold pads are used as contacts. You can see two types of wires soldered to chip offered by LakeShore in Figure 2.7. The chip on the left-hand side is CX-BG type with two gold lead wires and on the right-hand side is CX-BC type with two copper lead wires.

The calculation of the radiative heat flow Q_R between the hot plate and temperature sensor is done for the bare chip without considering wires. The Stefan-Boltzmann law with radiative heat transfer coefficient measured by us (eq. 2.3 and 2.4) was used for

(a) CX-BG type   **(b)** CX-BC type
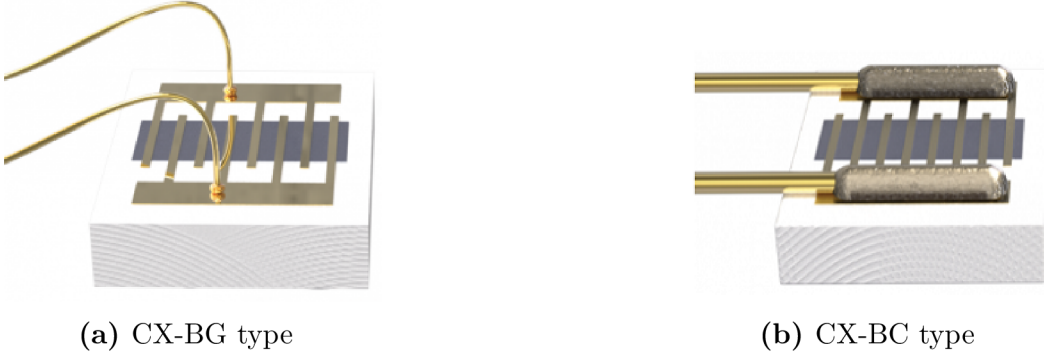
Figure 2.7: Two types of bonding of wires to both contact pads of the Cernox® thin film resistance cryogenic temperature sensors. In Figure (a), CX-BG type with the wires made of gold. In Figure (b), there is CX-BC type with the wires made of copper. Adapted from [17]

calculations. The temperatures T_1 and T_2 represent the temperatures of the bottom hot plate and the sensor, respectively. They were selected from the experimental data measured by Urban et al. at ISI in Brno [38]. The biggest temperature $T_2 = 6.5$K and the temperature difference between the plates $\Delta T = 1.8$ K among the data were chosen with an intention to find the biggest influence of thermal radiation but still to simulate an experiment by working with real data.

Results are then compared with self-heating (power dissipation) of the sensor which is $Q_{SH} = 10^{-7}$ W at 4.2 K at recommended excitation. This value is given by manufactures and should keep the temperature rise of the sensor below 1 mK.
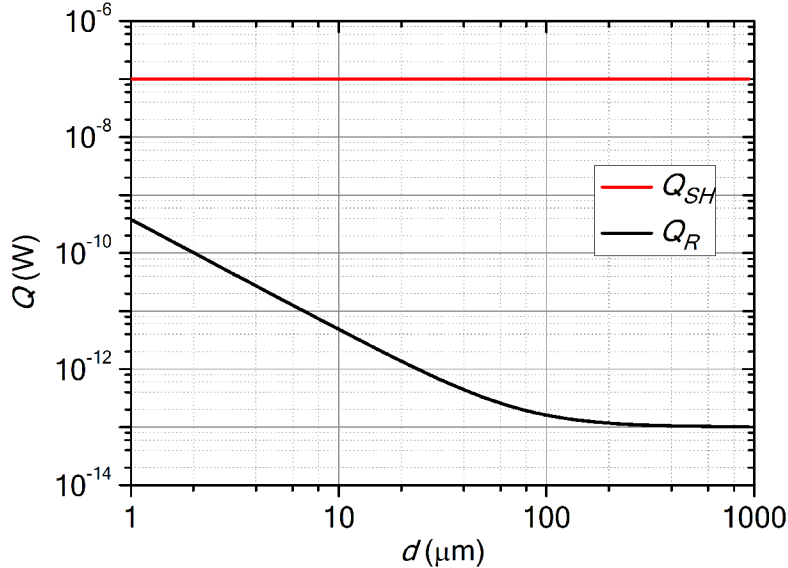
Figure 2.8: Comparison of the self-heating (power dissipation) of the Cernox® sensor (red line) at 4.2 K with the heat flow Q_R (black line) transferred by thermal radiation between the hot bottom plate and the sensor in the cryogenic experimental cell for RBC study for. The temperatures of the plate $T_2 = 6.5$ K and sensor $T_1 = 4.7$ K) are supposed to be constant for variable distance d between of them.

22

Another sensor is Ge-on-GaAs film resistance thermometer, especially model TTR-G, by the MicroSensor company [5]. This sensor is also stable in strong magnetic fields. It can operate in a range of temperatures 0.3 to 400 K.

Evaporation of Ge in a vacuum onto semi-insulating GaAs substrates was used for deposition. Contacts are made of Au and GeAu layers sometimes with Mo interlayer between them. Whole design of sensor is in Figure 2.9a. The chip is 0.3 mm wide, 0.3 mm long and 0.2 mm high. This is also offered in many packages. In the study of BLs, the bare chip is better to use. Photo of the bare chip is in Figure 2.9b. This chip was used in the RBC experiments at the Institute of Scientific Instruments in Brno.
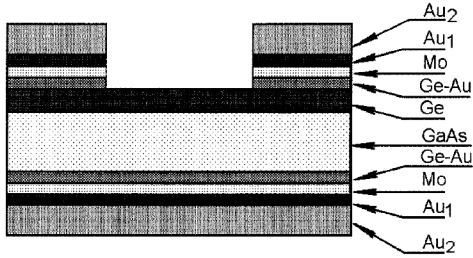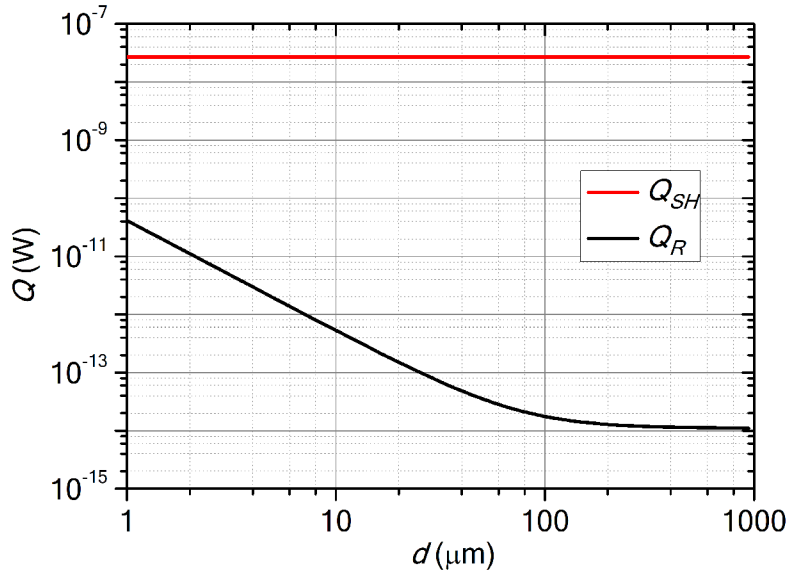

(a) Design of Ge/GaAs sensor
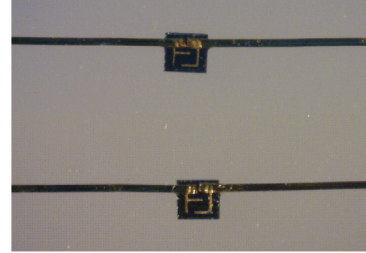
(b) Photo of two identical Ge/GaAs sensors

Figure 2.9: Scheme of Ge-film sensitive element temperature sensor and photo of bare Ge-on-GaAs chip [5]

The calculation for this sensor is similar as above but with different size of the chip. Self-heating of Ge/GaAs sensor is not defined by the producer. In this case, the equation for joule heating $Q_{SH} = RI^2$ is used. Normal operating current is $I = 3\,\mu A$ and resistance is defined by the producer. For our range of temperatures, the resistance is approximately $R = 3\,k\Omega$. This gives us the value $Q_{SH} = 2.7 \cdot 10^{-8}\,W$. The results are in Figure 2.10.

There are two and more orders of magnitude difference between the power dissipation Q_{SH} of the sensor and the heat transferred by thermal radiation Q_R for both sensors. In all calculations, the same temperature difference $\Delta = 1.8\,K$ was kept as a pessimistic assessment of the NF effect. When we consider the linear temperature profile of the BL, the heat transfer by radiation is even lower.

As I said above, the rise of the temperature due to self-heating caused by Joule heating should be below 1 mK. The power transferred by thermal radiation is lower than this value and would not affect the measurement of the temperature with both types of sensors, as is shown in Figures 2.8 and 2.10.

Figure 2.10: Self-heating (power dissipation) Q_{SH} of Ge/GaAs sensor (red line) calculated as Joule heating $Q_{SH} = RI^2$ and the heat flow Q_R (black line) transferred by thermal radiation initiating from the plate of the experimental cell for RBC study. The temperatures of the plate $T_2 = 6.5\,\mathrm{K}$ and sensor $T_1 = 4.7\,\mathrm{K}$) are supposed to be constant for variable distance d between of them.

2.4. Comparison of the radiative heat transfer with the convective heat transfer

In this last section, we compare the radiative heat flow Q_R with the total heat flow Q_t. The data from Brno, Grenoble, and Trieste presented in Figure 1.6 are used. Above in section 2.3, we have already calculated the thicknesses of the thermal BLs for these experiments. These thicknesses are used for the calculation of the radiative heat flow Q_R. The calculated values are just theoretical because, at a given distance, NF heat transfer from the hot plate will be strongest, when the absorbing surface has the same optical properties, it means maximum heat transfer from Cu to Cu plate. The results of radiative heat flow Q_R are what would be transferred if the second plate was at the end of BL. The results are in Figure 2.11 compared with the total heat flow Q_t already measured by the different scientific groups [26, 31, 39].

Again, there is a big order of magnitude difference: five and more orders of magnitude. So, we can surely say, that the heat flow by thermal radiation over the BLs is negligibly small in comparison with the convective heat flow. We can conclude that NF effect does not explain the controversy in heat transfer efficiency observed at high Ra numbers in different cryogenic experiments (see Figure 1.6), especially the crossover to to the ultimate regime claimed by Grenoble group.
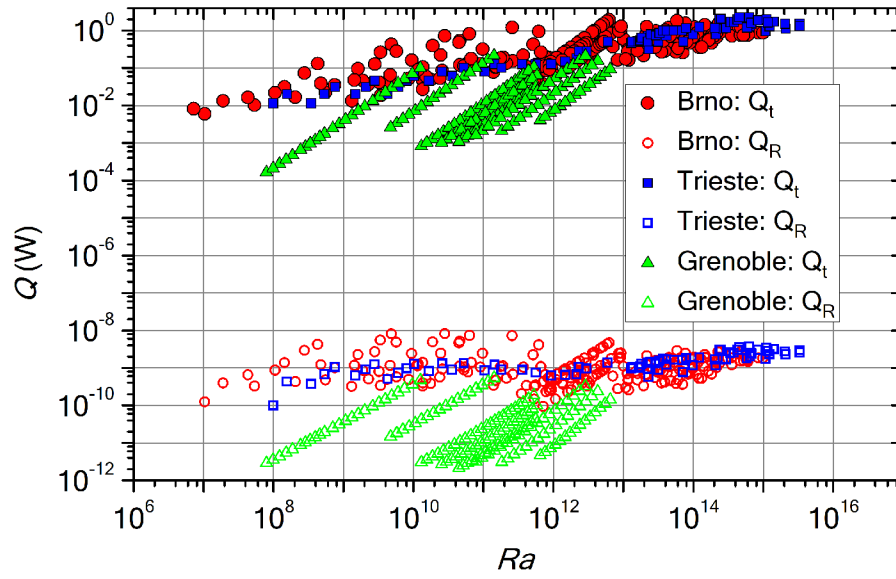
Figure 2.11: Comparison of the radiative heat flow Q_R with the total heat flow Q_t evaluated for the data sets of three cryogenic experiments from Brno, Grenoble and Trieste presented in Figure 1.6

3. Summary and conclusions

Firstly, the measurements of thermal radiation between two plane parallel Cu plates over microscopic distances at cryogenic temperatures are presented. The measurements were done with evanescent wave apparatus designed and assembled at the Institute of Scientific Instruments in Brno. Then the dependence of the coefficient of radiative heat transfer on the product of temperature and distance was fitted on the data from the experiment. This is shown in Figure 2.3 and the model is given by Eq. 2.3.

The coefficient of radiative heat transfer found is then used in the Stefan-Boltzmann law to evaluate the effect on different issues associated with Rayleigh-Bénard convection, namely (i) the onset of convection, (ii) thermal influence on temperature sensors and (iii) comparison with convective heat transfer and heat transfer efficiency at high Rayleigh numbers.

The effect of the thermal near field was studied for the experiment made by M. Lees et al. [18], scrutinizing their values of critical Rayleigh numbers Ra_c. Their values of Ra_c were above theoretical value and raised with increasing temperature. Dimensions of their experimental cell and temperature range make us think about the near field influence. The heat flows by conduction and by thermal near field are then calculated for this experiment. The results in Figure 2.4 show us the several orders of magnitude difference between heat power transferred by near field and by conduction. This allows us to say that there is no effect of the thermal near field on the onset of convection.

The second topic of our study was to evaluate the effect of the thermal near field on the sensors used for temperature profile measurements. Two sensors produced by two different companies were considered. First was Cernox® made by the LakeShore company. The second one was Ge-on-GaAs film resistance thermometer, TTR-G model, made by the MicroSensor company. At the beginning of this part, the thicknesses of thermal boundary layers are calculated to know the range of distances where we have to put the sensors to study their temperature profile (see Figure 2.5). The calculated heat flow from the thermal near field is then compared with power dissipation due to self-heating of the sensors. The results for Cernox® are in Figure 2.8 and for TTR-G model in Figure 2.10. Here, the difference is not as big as above, but when we take into the consideration the fact, that the rise of the temperature due to self-heating should be below $1\,\mathrm{mK}$, and our calculated heat flow is more than hundred times smaller, we can say, that the thermal near field will not affect these sensors.

In the last section, the radiative heat flow over distances corresponding to the thicknesses of thermal boundary layers is compared with convective heat flow observed in different cryogenic experiments at high Rayleigh numbers. Here the gap between them is huge, five and more orders of magnitude, so the effect of the thermal near field is negligibly small in comparison with the convective heat flow and we don't have to take it into the considerations as the parasitic effect in RBC studies.

In conclusion, we have performed detailed measurements and analysis of possible 'parasitic' effects of radiative heat transfer on measurements of conductive and convective heat transfer in Rayleigh Benard convection. Apriori, the the effects in low temperature helium experiments in cells with copper plates cannot be simply neglected, especially as the relevant spatial scales (of the RBC boundary layers or cell heights) are within the reach of thermal near field, which greatly supersedes the usual far field radiation given by Planck's law. Nevertheless our analysis has clarified that the effects can be neglected justly. The

results are relevant for future RBC experiments aimed at the so-called ultimate regime of turbulent RBC [14, 37] intensely studied in numerous laboratories worldwide [2].

Bibliography

[1] AHLERS, Guenter, Eberhard BODENSCHATZ, Denis FUNFSCHILLING, Siegfried GROSSMANN, Xiaozhou HE, Detlef LOHSE, Richard J. A. M. STEVENS a Roberto VERZICCO. Logarithmic Temperature Profiles in Turbulent Rayleigh-Bénard Convection. *Physical Review Letters* [online]. 2012, **109**(11) [cit. 2019-04-01]. DOI: 10.1103/PhysRevLett.109.114501. ISSN 0031-9007. Available at: https://link.aps.org/doi/10.1103/PhysRevLett.109.114501

[2] AHLERS, Guenter, Siegfried GROSSMANN and Detlef LOHSE. 2009. Heat transfer and large scale dynamics in turbulent Rayleigh-Bénard convection. *Reviews of Modern Physics* [online]. 2009, **81**(2), 503-537 [cit. 2019-04-22]. DOI: 10.1103/RevModPhys.81.503. ISSN 0034-6861. Available at: https://link.aps.org/doi/10.1103/RevModPhys.81.503

[3] BARENGHI, Carlo F., Chris J. SWANSON and Russell J. DONNELLY. 1995. Emerging issues in helium turbulence. *Journal of Low Temperature Physics* [online]. 1995, **100**(5-6), 385-413 [cit. 2019-04-01]. DOI: 10.1007/BF00751517. ISSN 0022-2291. Available at: http://link.springer.com/10.1007/BF00751517

[4] BODENSCHATZ, Eberhard, Werner PESCH and Guenter AHLERS. 2000. Recent Developments in Rayleigh-Bénard Convection. *Annual Review of Fluid Mechanics* [online]. 2000, **32**(1), 709-778. 709-778 [cit. 2019-05-01]. DOI: 10.1146/annurev.fluid.32.1.709. ISSN 0066-4189. Available at: http://www.annual-reviews.org/doi/10.1146/annurev.fluid.32.1.709

[5] BOLTOVETS, N.S., V.V. KHOLEVCHUK, R.V. KONAKOVA, V.F. MITIN and E.F. VENGER. 2000. Ge-film resistance and Si-based diode temperature microsensors. In: *ASDAM 2000. Conference Proceedings. Third International EuroConference on Advanced Semiconductor Devices and Microsystems (Cat. No.00EX386)* [online]. IEEE, 2000, p. 235-238 [cit. 2019-04-29]. DOI: 10.1109/ASDAM.2000.889489. ISBN 0-7803-5939-9. Available at: http://ieeexplore.ieee.org/document/889489/

[6] CASTAING, Bernard, Gemunu GUNARATNE, François HESLOT, et al. 1989. Scaling of hard thermal turbulence in Rayleigh-Bénard convection. *Journal of Fluid Mechanics* [online]. 1989, **204**(-1) [cit. 2019-05-08]. DOI: 10.1017/S0022112089001643. ISSN 0022-1120. Available at: http://www.journals.cambridge.org/abstract_S0022112089001643

[7] CHANDRASEKHAR, S. *Hydrodynamic and hydromagnetic stability.* Dover ed. New York: Dover Publications, 1961. International series of monographs on physics (Oxford, England). ISBN 048664071x.

[8] CHARLSON, G.S and R.L SANI. Thermoconvective instability in a bounded cylindrical fluid layer. *International Journal of Heat and Mass Transfer* [online]. 1970, **13**(9), 1479-1496 [cit. 2019-03-15]. DOI: 10.1016/0017-9310(70)90181-X. ISSN 00179310. Available at: https://linkinghub.elsevier.com/retrieve/pii/001793107090181X

[9] CHAVANNE, X., F. CHILLÀ, B. CHABAUD, B. CASTAING, J. CHAUSSY and B. HÉBRAL. High rayleigh number convection with gaseous helium at low temperature. *Journal of Low Temperature Physics* [online]. 1996, **104**(1-2), 109-129 [cit. 2019-04-22]. DOI: 10.1007/BF00754092. ISSN 0022-2291. Available at: http://link.springer.com/10.1007/BF00754092

[10] CHILLÀ, F. and J. SCHUMACHER. New perspectives in turbulent Rayleigh-Bénard convection. *The European Physical Journal E* [online]. 2012, **35**(7) [cit. 2019-03-15]. DOI: 10.1140/epje/i2012-12058-1. ISSN 1292-8941. Available at: http://link.springer.com/10.1140/epje/i2012-12058-1

[11] CROSS, M. C. and P. C. HOHENBERG. Pattern formation outside of equilibrium. *Reviews of Modern Physics* [online]. 1993, **65**(3), 851-1112 [cit. 2019-04-27]. DOI: 10.1103/RevModPhys.65.851. ISSN 0034-6861. Available at: https://link.aps.org/doi/10.1103/RevModPhys.65.851

[12] DRAHOTSKY, Jakub. Temperature profiles and temperature fluctuations in turbulent Rayleigh-Bénard convection: master's thesis. Brno: Brno University of Technology, Faculty of Mechanical Engineering, Institute of Physical Engineering, 2018. 69 p. Supervised by Ing. Pavel Urban, Ph.D.

[13] GAO, H., G. METCALFE, T. JUNG and R. P. BEHRINGER. Heat-flow experiments in liquid 4 He with a variable cylindrical geometry. *Journal of Fluid Mechanics* [online]. 1987, **174**(-1) [cit. 2019-04-15]. DOI: 10.1017/S0022112087000107. ISSN 0022-1120. Available at: http://www.journals.cambridge.org/abstract_S0022112087000107

[14] KRAICHNAN, Robert H. Turbulent Thermal Convection at Arbitrary Prandtl Number. *Physics of Fluids* [online]. 1962, **5**(11) [cit. 2019-05-08]. DOI: 10.1063/1.1706533. ISSN 00319171. Available at: https://aip.scitation.org/doi/10.1063/1.1706533

[15] KRALIK, Tomas, Pavel HANZELKA, Martin ZOBAC, Vera MUSILOVA, Tomas FORT and Michal HORAK. Strong Near-Field Enhancement of Radiative Heat Transfer between Metallic Surfaces. *Physical Review Letters* [online]. 2012, **109**(22) [cit. 2019-03-16]. DOI: 10.1103/PhysRevLett.109.224302. ISSN 0031-9007. Available at: https://link.aps.org/doi/10.1103/PhysRevLett.109.224302

[16] KRALIK, T., P. HANZELKA, V. MUSILOVA, A. SRNKA and M. ZOBAC. Cryogenic apparatus for study of near-field heat transfer. *Review of Scientific Instruments* [online]. 2011, **82**(5) [cit. 2019-03-15]. DOI: 10.1063/1.3585985. ISSN 0034-6748. Available at: http://aip.scitation.org/doi/10.1063/1.3585985

[17] *Lake Shore Cryotronics, Inc.* [online]. c1996, last revision 19th of April [cit. 2019-05-09]. <https://www.lakeshore.com>.

[18] LEES, Matthew J., Michael S. THURLOW, James R. T. SEDDON and Peter G. J. LUCAS. Critical Rayleigh Number Controversy For Liquid 4He. In: *AIP Conference Proceedings* [online]. AIP, 2006, 2006, p. 153-154 [cit. 2019-03-16]. DOI: 10.1063/1.2354648. ISSN 0094243X. Available at: http://aip.scitation.org/doi/abs/10.1063/1.2354648

[19] LEES, Matthew J., Michael S. THURLOW, James R. T. SEDDON a Peter G. J. LUCAS. Convective Roll Dynamics in Liquid H e 4 near the Onset of Convection. *Physical Review Letters* [online]. 2004, **93**(14) [cit. 2019-05-08]. DOI: 10.1103/PhysRevLett.93.144502. ISSN 0031-9007. Available at: https://link.aps.org/doi/10.1103/PhysRevLett.93.144502

[20] LEES, Matthew J.: Visualising Flow pattern Instabilities in Low Temperature Convection. [Ph.D. Thesis], University of Manchester, 2003

[21] LI, K.R., G. ZHOU, L.Q. LIU, L.Y. XIONG, B. DONG, Z.Y. LI and Q. LI. Reducing the Uncertainty of Self-heating in High-accuracy Cryogenic Temperature Measurements. *Physics Procedia* [online]. 2015, **67**, 1157-1163 [cit. 2019-04-28]. DOI: 10.1016/j.phpro.2015.06.180. ISSN 18753892. Available at: https://linkinghub.elsevier.com/retrieve/pii/S1875389215005611

[22] LOOMIS, Jackson J. and Humphrey J. MARIS. Theory of heat transfer by evanescent electromagnetic waves. *Physical Review B* [online]. 1994, **50**(24), 18517-18524 [cit. 2019-03-15]. DOI: 10.1103/PhysRevB.50.18517. ISSN 0163-1829. Available at: https://link.aps.org/doi/10.1103/PhysRevB.50.18517

[23] MALKUS, W. V. R. The heat transport and spectrum of thermal turbulence. *Proceedings of the Royal Society of London. Series A. Mathematical and Physical Sciences* [online]. 1954, **225**(1161), 196-212 [cit. 2019-05-05]. DOI: 10.1098/rspa.1954.0197. ISSN 2053-9169. Available at: http://www.royalsocietypublishing.org/doi/10.1098/rspa.1954.0197

[24] METCALFE, G. P. and R. P. BEHRINGER. Critical Rayleigh numbers for cryogenic experiments. *Journal of Low Temperature Physics* [online]. 1990, **78**(3-4), 231-246 [cit. 2019-04-01]. DOI: 10.1007/BF00686102. ISSN 0022-2291. Available at: http://link.springer.com/10.1007/BF00686102

[25] MUSILOVÁ, Věra, Tomáš KRÁLÍK, Tomáš FOŘT and Michal MACEK. Strong suppression of near-field radiative heat transfer by superconductivity in NbN. *Physical Review B* [online]. 2019, **99**(2) [cit. 2019-04-24]. DOI: 10.1103/PhysRevB.99.024511. ISSN 2469-9950. Available at: https://link.aps.org/doi/10.1103/PhysRevB.99.024511

[26] NIEMELA, J. J. and K. R. SREENIVASAN. Confined turbulent convection. *Journal of Fluid Mechanics* [online]. 2002, **481**, 355-384 [cit. 2019-04-22]. DOI: 10.1017/S0022112003004087. ISSN 00221120. Available at: http://www.journals.cambridge.org/abstract_ S0022112003004087

[27] NIEMELA, J. J., L. SKRBEK, K. R. SREENIVASAN a R. J. DONNELLY. Turbulent convection at very high Rayleigh numbers. *Nature* [online]. 2000, **404**(6780), 837-840 [cit. 2019-05-09]. DOI: 10.1038/35009036. ISSN 0028-0836. Available at: http://www.nature.com/articles/35009036

[28] PENDRY, J B. Radiative exchange of heat between nanostructures. *Journal of Physics: Condensed Matter* [online].

1999, **11**(35), 6621-6633 [cit. 2019-04-08]. DOI: 10.1088/0953-8984/11/35/301. ISSN 0953-8984. Available at: http://stacks.iop.org/0953-8984/11/i=35/a=301?key=crossref.e1b24dc8e8a22b7a42b7bcf46525ac37

[29] POLDER, D. and M. VAN HOVE. Theory of Radiative Heat Transfer between Closely Spaced Bodies. *Physical Review B* [online]. 1971, 4(10), 3303-3314 [cit. 2019-03-15]. DOI: 10.1103/PhysRevB.4.3303. ISSN 0556-2805. Available at: https://link.aps.org/doi/10.1103/PhysRevB.4.3303

[30] RIDOUANE, E. H., M. HASNAOUI, A. AMAHMID a A. RAJI. INTERACTION BETWEEN NATURAL CONVECTION AND RADIATION IN A SQUARE CAVITY HEATED FROM BELOW. *Numerical Heat Transfer, Part A: Applications* [online]. 2004, **45**(3), 289-311 [cit. 2019-05-01]. DOI: 10.1080/10407780490250373. ISSN 1040-7782. Available at: http://www.tandfonline.com/doi/abs/10.1080/10407780490250373

[31] ROCHE, P-E, F GAUTHIER, R KAISER a J SALORT. On the triggering of the Ultimate Regime of convection. *New Journal of Physics* [online]. 2010, **12**(8) [cit. 2019-05-08]. DOI: 10.1088/1367-2630/12/8/085014. ISSN 1367-2630. Available at: http://stacks.iop.org/1367-2630/12/i=8/a=085014?key=crossref.ad7a0b9190332a738a48323b7670dea5

[32] SCHÜTZ, S and E BODENSCHATZ. Two-particle dispersion in weakly turbulent thermal convection. *New Journal of Physics* [online]. 2016, **18**(6) [cit. 2019-04-29]. DOI: 10.1088/1367-2630/18/6/065007. ISSN 1367-2630. Available at: http://stacks.iop.org/1367-2630/18/i=6/a=065007?key=crossref.4ddff00a772d609f7605f1f6a5720182

[33] SHRAIMAN, Boris I. a Eric D. SIGGIA. Heat transport in high-Rayleigh-number convection. *Physical Review A* [online]. 1990, **42**(6), 3650-3653 [cit. 2019-05-08]. DOI: 10.1103/PhysRevA.42.3650. ISSN 1050-2947. Available at: https://link.aps.org/doi/10.1103/PhysRevA.42.3650

[34] SKRBEK, L. a P. URBAN. Has the ultimate state of turbulent thermal convection been observed?. *Journal of Fluid Mechanics* [online]. 2015, **785**, 270-282 [cit. 2019-05-09]. DOI: 10.1017/jfm.2015.638. ISSN 0022-1120. Available at: http://www.journals.cambridge.org/abstract_ S0022112015006382

[35] SREENIVASAN, Katepalli R. and Russell J. DONNELLY. Role of cryogenic helium in classical fluid dynamics: Basic research and model testing. *Advances in Applied Mechanics Volume 37* [online]. Elsevier, 2001, 2001, p. 239-276 [cit. 2019-04-01]. Advances in Applied Mechanics. DOI: 10.1016/S0065-2156(00)80007-1. ISBN 9780120020379. Available at: https://linkinghub.elsevier.com/retrieve/pii/S0065215600800071

[36] SUN, Hua, Eric CHÉNIER a Guy LAURIAT. Effect of surface radiation on the breakdown of steady natural convection flows in a square, air-filled cavity containing a centered inner body. *Applied Thermal Engineering* [online]. 2011, **31**(6-7), 1252-1262 [cit. 2019-05-01]. DOI: 10.1016/j.applthermaleng.2010.12.028. ISSN 13594311. Available at: https://linkinghub.elsevier.com/retrieve/pii/S1359431110005442

[37] URBAN, P., P. HANZELKA, T. KRÁLÍK, M. MACEK, V. MUSILOVÁ a L. SKRBEK. Elusive transition to the ultimate regime of turbulent Rayleigh-Bénard convection. *Physical Review E* [online]. 2019, **99**(1) [cit. 2019-05-09]. DOI: 10.1103/PhysRevE.99.011101. ISSN 2470-0045. Available at: https://link.aps.org/doi/10.1103/PhysRevE.99.011101

[38] URBAN, Pavel, Pavel HANZELKA, Věra MUSILOVÁ, Tomáš KRÁLÍK, Marco La MANTIA, Aleš SRNKA and Ladislav SKRBEK. Heat transfer in cryogenic helium gas by turbulent Rayleigh–Bénard convection in a cylindrical cell of aspect ratio 1. *New Journal of Physics* [online]. 2014, **16**(5) [cit. 2019-04-22]. DOI: 10.1088/1367-2630/16/5/053042. ISSN 1367-2630. Available at: http://stacks.iop.org/1367-2630/16/i=5/a=053042?key=crossref.3333726bedc224db37943381a48d6f5d

[39] URBAN, P., P. HANZELKA, T. KRALIK, V. MUSILOVA, A. SRNKA and L. SKRBEK. Effect of Boundary Layers Asymmetry on Heat Transfer Efficiency in Turbulent Rayleigh-Bénard Convection at Very High Rayleigh Numbers. *Physical Review Letters* [online]. 2012, **109**(15) [cit. 2019-04-20]. DOI: 10.1103/PhysRevLett.109.154301. ISSN 0031-9007. Available at: https://link.aps.org/doi/10.1103/PhysRevLett.109.154301

[40] WANG, Yuancheng, Jun YANG, Xiaojing ZHANG a Yu PAN. Effect of Surface Thermal Radiation on Natural Convection and Heat Transfer in a Cavity Containing a Horizontal Porous Layer. *Procedia Engineering* [online]. 2015, **121**, 1193-1199 [cit. 2019-05-01]. DOI: 10.1016/j.proeng.2015.09.137. ISSN 18777058. Available at: https://linkinghub.elsevier.com/retrieve/pii/S1877705815029653

List of symbols, physical constants and abbreviations

σ	Stefan-Boltzmann constant ($\mathrm{Wm^{-2}K^{-4}}$)
c_0	velocity of light in free space ($\mathrm{ms^{-1}}$
$\hbar$	reduced Planck constant (Js)
k_B	Boltzmann constant ($\mathrm{J{\cdot}K^{-1}}$)
Γ	Aspect ratio (-)
Ra	Rayleigh number (-)
Ra_c	Critical Rayleigh number (-)
Pr	Prandtl number (-)
Nu	Nusselt number (-)
D	Diameter of the cell (m)
L	Height of the cell (m)
g	Gravitational acceleration ($\mathrm{ms^{-2}}$)
α	Coefficient of thermal expansion (1/K)
ν	Kinematic viscosity ($\mathrm{mm^2/s}$)
κ	Thermal diffusivity ($\mathrm{mm^2/s}$)
Q_t	Total heat flow (W)
Q_λ	Conductive heat flow (W)
S	Area of the surface ($\mathrm{m^2}$)
λ	Thermal conductivity (mW/m·K)
λ_{BL}	Thickness of the thermal boundary layer (μm)
Q_{BB}	Radiative heat flow from Black body (W)
Q_R	Radiative heat flow (W)
Q_{HA}	Heat flow from the calibration heater (W)
T	Temperature (K)
T_0	Temperature of the theraml stabilization (K)
T_1	Temperature of the colder object (absorber in the apparatus) (K)

T_2	Temperature of the hotter object (emitter in the apparatus) (K)
T_m	Mid-plane temperature (K)
d	Distance between the objects (μm)
δQ_R	Total uncertainty of the measured heat flow Q_R (W, %)
$T_{0,res}$	Resolution of the temperature measurements of T_0
$T_{1,res}$	Resolution of the temperature measurements of T_1
Q_{SH}	Thermal dissipation due to self-heating of the sensor (W)
R	Resistance (Ω)
I	Current (A)
ISI	Institute of Scientific Instruments
LHe	Liquid Helium
LN$_2$	Liquid Nitrogen
RBC	Rayleigh-Bénard convection
BL	Boundary Layer
EWA	Evanescent wave apparatus
NF	Near field
FF	Far field